Utility of optical heterodyne displacement sensing and laser ultrasonics as *in situ* process control diagnostic for additive manufacturing

Anthony J. Manzo
Henry Helvajian

SPIE.

Utility of optical heterodyne displacement sensing and laser ultrasonics as *in situ* process control diagnostic for additive manufacturing

Anthony J. Manzo and Henry Helvajian*
The Aerospace Corporation, Physical Sciences Laboratories, Los Angeles, California, United States

Abstract. An *in situ* process control monitor is presented by way of experimental results and simulations, which utilizes a pulsed laser ultrasonic source as a probe and an optical heterodyne displacement meter as a sensor. The intent is for a process control system that operates in near real time, is nonintrusive, and *in situ*: A necessary requirement for a serial manufacturing technology such as additive manufacturing (AM). We show that the diagnostic approach has utility in characterizing the local temperature, the area of the heat-affected zone, and the surface roughness ($R_a \sim 0.4~\mu$m). We further demonstrate that it can be used to identify solitary defects (i.e., holes) on the order of 10 to 20 μm in diameter. Moreover, the technique shows promise in measuring properties of materials with features that have a small radius of curvature. We present results for a thin wire of ~650 μm in diameter. By applying multiple pairs of probe–sensor systems, the diagnostic could also measure the local cooling rate on the scale of 1 μs. Finally, while an obvious application is used in AM technology, then all optical diagnostics could be applied to other manufacturing technologies. © *The Authors. Published by SPIE under a Creative Commons Attribution 3.0 Unported License. Distribution or reproduction of this work in whole or in part requires full attribution of the original publication, including its DOI.* [DOI: 10.1117/1.OE.57.4.041415]

1 Introduction

Additive manufacturing (AM) is a promising technology that produces working parts out of metals, polymers, and composites. The desirable attributes of AM include the direct fabrication of complex three-dimensional (3-D) shapes and the potential to produce parts with tailored material properties. Current AM methods include the use of a laser or electron beam to melt and fuse stock material that is delivered as a powder through a jet nozzle, dispensed as a powder bed with repeated layering, as a thin spool of wire that is just unreeled, or a vat of material with photolytic cross-linking properties that harden upon focused laser irradiation. A more ubiquitous method in the case of polymer material is a fabrication approach that extrudes stock material in a continuous layer formation process. Metal extrusion methods are also used in the development[1–3] along with techniques that deposit a powder form of a material, layer-by-layer, within a sacrificial powder host and the whole object is heated to selectively sinter the material within the host.[4,5] All these techniques have advantages and shortcomings with the primary shortcoming being poor process control. Process control could be based on a low fidelity diagnostic if the parts produced are just prototypes. However, in the past decade there has been a drive to fabricate production parts on AM tools that have heritage from prototype processing. One envisions more process control diagnostics in the next generation AM tools.

In situ diagnostics have an advantage over *ex situ* and this is especially significant in AM because of the serial nature of the fabrication and the ability to take corrective action (i.e., stop or fix) when the process has gone askew. For example, the "midstream" identification of a location, where there has been improper sintering, might initiate a quick ancillary process that provides additional local heat. This form of corrective action is only possible when the diagnostic is *in situ*. *In situ* diagnostics for AM can be realized in different ways, but optical imaging and spectroscopy of the imaged region are the easiest because they are not intrusive to the manufacturing process.

Current state of the art for *in situ* monitoring and process control in AM is evolving[6–8] and variations exist between powder bed diffusion processes (where melting occurs at a work site in a powder bed) and directed energy deposition (DED) processes (where the material is melted as deposited). Temperature, melt pool size, geometry, and melt pool dynamics are some of the main process parameters of interest that determine product quality. Common sensors to monitor these parameters include photodetectors, CMOS cameras, IR cameras, and pyrometers. Photodetectors and cameras are often used to measure, with varying success and strongly dependent upon the setup, the melt pool sizes, temperatures, solidification rates, and structural geometries. Pyrometers are usually used to measure temperatures. These sensors are most effectively utilized in conjunction with data analysis and feedback control mechanisms. Data from sensors can also be analyzed to indirectly characterize other properties such as residual stress.

Although these sensors and techniques do have their advantages, they fail in the following respects: (1) They

*Address all correspondence to: Henry Helvajian, E-mail: Henry.Helvajian@Aero.org

"sample" only the surface area and cannot "probe" the layer below (e.g., 20 to 50 μm); (2) The use of imaging for the thermal analysis requires accurate knowledge of material emissivity—emissivity is very sensitive to the shape of the formed structure size and in AM this can vary throughout a build (to some extent depending on the amount of material or thermal sink is adjoining); and (3) Optical spectroscopy of the emission (surface or above surface, e.g., sparks) will be even more sensitive to the applied local energy flux that is guaranteed to vary during patterning because of the inertia in the motion platform. A solution to this third problem, which surprisingly has not been implemented, is the synchronous amplitude modulation of the laser/energy source with the motion platform.[9] Moreover, the development of an optical spectroscopy system can be complex if information on the scale of tens of microns is necessary from a distance of tens centimeters.

One possible *in situ* diagnostic, which is described in this report, merges the power of optical techniques with that of ultrasound, which can penetrate even refractory materials. We present the development of an *in situ* monitoring diagnostic that could be used as a process control for laser-AM. The technique applies two low-power lasers that can be focused to within microns of the region of interest, if necessary. One laser is the initiator or probe and generates wide broadband ultrasound ($\Delta\nu > 100$ MHz). The second serves as the sensor measuring, by laser heterodyne spectroscopy, the displacement of the surface on the scale of nanometers. The time-resolved measured signal appears to track several parameters that are of interest to metallurgists. The technique can be implemented into existing AM tools with minimal modification.

The prominent ultrasonic wave mode that is excited and detected with our technique is the surface acoustic wave (SAW) or Rayleigh wave.[10,11] This mode propagates along the surface and is composed of a coupled shear and longitudinal wave. The velocity, V, of these dispersionless SAWs in materials can be described by the equations

$$V = \left[\frac{0.87 + 1.12\sigma}{1 + \sigma} \right] V_s, \tag{1}$$

$$\sigma = \frac{\left[1 - 2\left(\frac{V_s}{V_l}\right)^2 \right]}{2\left[1 - \left(\frac{V_s}{V_l}\right)^2 \right]}, \tag{2}$$

where σ is the Poisson ratio that relates to elastic properties of the material, V_s is the shear wave velocity, and V_l is the longitudinal wave velocity, respectively. The relation between the wavelength, Λ, and frequency, f, for a velocity is given by $\sim V/f$. For an SAW velocity of 3100 m/s in titanium alloy Ti6Al4V, a wave with frequency of 50 MHz will have a wavelength of 62 μm. Penetration depths of the SAW are approximately one or two times the wavelength, allowing the SAW to probe the layers of an AM build, which is typically a layer-by-layer process. The ability to measure the velocity of SAWs allows for the determination of elastic properties and tracking of other physical properties, such as temperature.[11,12] The modulus defines the mechanical properties in most materials, such as the velocity of sound

(typically 3 to 5 km/s for metals), and is temperature-dependent. An increase in the temperature typically decreases velocities of bulk waves and SAWs.[12,13] SAWs may also be measured and analyzed to infer frequency (wavelength) content, making it possible to gain information about additional properties, such as roughness, grain size, or defects related to microstructure.[14–17] SAWs in this work are generated from the thermoelastic response of the material with a laser pulse.[18] SAWs produced by laser pulses can have a higher frequency bandwidth than those generated with piezoelectric transducers. The higher bandwidth can be an advantage in certain measurements (see discussion below). The laser interferometer sensor used to measure surface displacements in this report allows for the recording and analysis of waves in broad frequency distributions.

Of the many diagnostic parameters thought to be necessary,[7] one is the need for monitoring the temperature at or near the sintering region as a function of time. The information establishes the possible alloy phases and the microstructure that could be present.[4,5,7,8] Some methods that have been employed, albeit not all, are *in situ*. The techniques include the use of interference of reflected light,[19] x-ray diffraction,[20] coherent Raman line shift spectroscopy,[21] thermionic emission,[22] time of flight,[23] ellipsometry,[24] and electron diffraction if crystalline phases are present,[25] and pyrometry.[26] Notwithstanding these techniques, we recently published a noncontact *in situ* approach that tracks the change in local temperature near a fusing/sintering zone. The technique is based on pulsed laser ultrasonic excitation and laser heterodyne interferometry.[27] The measured value is the change in the arrival time of the surface traveling ultrasonic wave (typically called an SAW). In this report, we further advance this diagnostic approach by presenting data that show (a) the ability to detect small surface defects (<20 μm), reminiscent of a feature left by an unmelted powder grain, (b) the utility to probe around shapes having small curvatures (e.g., a diagnostic for a wire fed AM tool), and (c) the ability to distinguish a roughened surface from a precalibrated norm on the scale of tens microns. The diagnostic technique that merges the capabilities of two nondestructive evaluation (NDE) disciplines (e.g., optical and ultrasound) does have the speed throughput that could even exceed some conventional or thermal[8] imaging techniques while providing more than one piece of information. Finally, it can also provide information from below the surface and is agnostic to the material and processing approach.

2 Experimental

The following proof-of-principle experiments were done on an automated XYZ stage and not within an AM tool. Figure 1 shows the general experimental setup with two different probe–sensor configurations. In one configuration depicted in the lower left of Fig. 1, three laser beams are directed onto a sample. The centrally located high-power processing or heating laser (representative of an AM processing laser) is accompanied by the probe laser on the one side, which generates short pulse SAWs by nonablative excitation and on the other side by the sensor laser that measures the surface displacement. The probe and sensor lasers are directed onto the sample via small (5 mm) prisms, with the probe prism coated for high reflectivity. The intent is positioning the probe and sensor lasers to be as close as
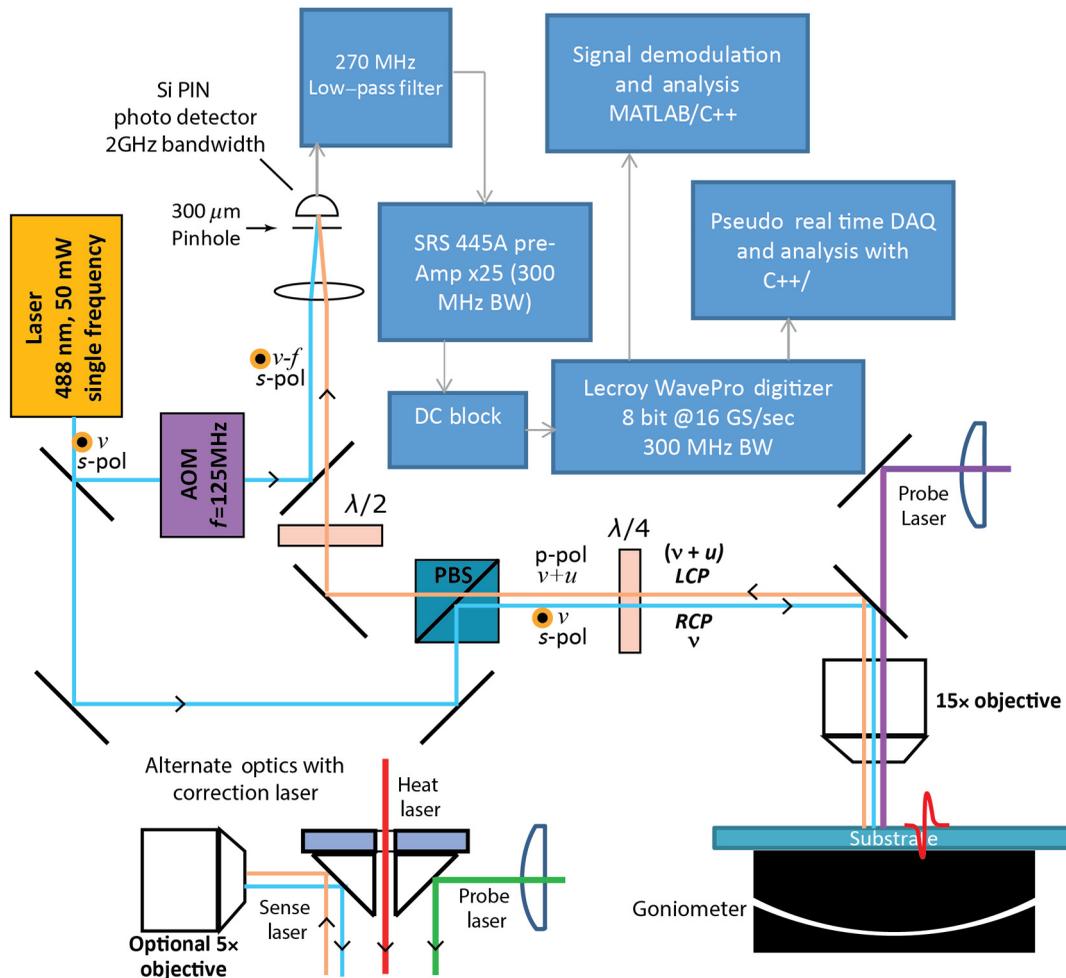
Fig. 1 Experimental setup. Shows schematic of optical heterodyne system, guiding assembly for laser beams onto substrate, and block diagram of data acquisition chain.

possible to the processing action. The second experimental configuration does not use a high-power laser but has the objective to measure surface roughness and detect solitary surface defects. In the second configuration, both probe and sensor laser beams are focused through the same single 15× objective lens (Thorlabs LMU-15X-UVB). This arrangement enables a shorter separation between the probe and sensor lasers (e.g., <100 μm) while also reducing the spot size of both the probe and sensor laser beams (e.g., <5 μm). Although the sensor laser focus produces a circular spot, the probe beam focal spot is typically rectangular, which helps in the generation of plane-wave SAWs. The sharp rectangular line at focus is made possible using a physical mask and a 10:1 optical image reduction telescope placed prior to the objective lens. The need for two experimental configurations is a direct result of our laboratory limitations. In an actual AM tool, configuration 2 would be used in which the three laser beams are delivered collinearly.

The sample is positioned by a computer-controlled XYZ motion stage (Aerotech A3200 motion controller), which also includes a tip-tilt goniometer (Thorlabs GN05). The XYZ motion stage is controlled by the Aerotech software, but MATLAB (with instrument drivers and Instrument control toolbox) and Python (using instrument drivers and pyVISA) are used to synchronize the motion platform

with the data acquisition system and the probe pulse initiation.

The surface displacement wave is digitized at 8 or 16 Gigasamples/s. The high-power processing laser (Coherent Innova Argon Ion) produces 20 W of CW output power when configured to operate on all laser lines (typically ~40% of 488 nm and ~60% of 514 nm). Before reaching the target, the high-power laser passes through a 5× objective (LMU-5X-UVB) forming an illuminated spot roughly 600 microns in diameter. The on-target laser power is measured by a Coherent PM10 power meter. Two probe lasers are used in the experiment

1. A pulsed, Q-switched (Coherent Evolution-30 Nd:YLF) green laser operating at 532-nm wavelength and repetition rate of 5 kHz. The 170-ns pulsewidth of the Nd:YLF laser is chopped to form a 60- or 40-ns pulse [full width at half maximum (FWHM)] by an electro-optic pulse slicer (Lasermetrics pulse gating system, 5046ER, with BBO crystal). The sliced pulse laser beam then passes through an anamorphic lens, (to compensate for differences in the divergence in the X- and Y-directions) and is focused by a 50- to 100-cm focal length cylindrical lens to form an approximate line shape on target with dimensions

of 100 μm × 5 mm. The average on-target power for the green probe laser is ∼1 W. The maximum single shot fluence produced is 40 mJ/cm^2, which is well below most damage thresholds for metals.[28]

2. A pulsed, *Q*-switched Nd-YAG (Spectra Physic QuantaRay, Lab-190) UV laser operating at 355-nm wavelength at a repetition rate of 100 Hz. The UV pulsed laser has a pulse width of 6 ns. The average on target power for the UV laser depends on the optical configuration and the material studied but ranges from 0.5 to tens of mW.

Although the Nd-YAG laser (200 W) may have been a suitable choice to use as a heating laser, at the time of the experiment, the safety protocols for the IR laser were not yet in place as it was for the visible laser.

The optical heterodyne system (Fig. 1) is based on a 488-nm CW narrow bandwidth laser (Coherent Sapphire 488 SF, 50-mW max power, 0.70 beam diameter ($1/e^2$), and line-width <1.5 MHz). The laser beam is split into two beams to form the reference and sensor arms. The reference arm passes through a 125-MHz acousto-optic modulator (AOM) (Brimrose TEF-125-50-488, 50-MHz bandwidth, Tellurium Dioxide, TeO$_2$, substrate with FFF-125-B2-F0.4-CO fixed frequency driver) and the −1 diffracted order from the AOM is used as the reference. The sensor arm is not modulated and directed on to the sample surface. The polarization of the incident and surface reflected laser beams is altered to keep the incident and reflected sensor beams from interfering. The reference and reflected sensor beams are then brought to a focus and made to overlap onto a photodetector (EOT-2020, 2 GHz), which is covered by a 300-μm pinhole. The photodetector signal is low-pass filtered (270 MHz), amplified (×25) by a 350-MHz bandwidth low-noise pre-amplifier (SRS 445A), and passes through a DC block filter. The signal is then digitized with 8-bit resolution by a sampling scope (Lecroy WavePro 960, 330 MHz bandwidth). To further enhance the on-target spatial accuracy of the sensor measurement, the heterodyne sensor beam is focused with a 5× objective (Thorlabs LMU-5X-UVB, NA = 0.13, working distance of 37.3 mm) and forms a spot ∼67 μm in diameter. The reflected light is collected by this same objective. The data acquisition is synchronized via a photodetector monitoring the probe laser. High-speed mechanical shutters (Uniblitz LS6Z2 and LS6S2ZM0, minimum open time of 700 μs, and VCM-D1 driver) are used to record data for a specific number of SAW pulses. Moreover, with software control and delay generators that drive the mechanical shutters, burst mode data acquisition becomes possible (i.e., 3 to 5 SAW pulse bursts of data are captured over a 0.5-s time interval).

The digitized data are processed and analyzed using software written in MATLAB and Python. A Hilbert transform is used to demodulate the signal to produce time-resolved surface displacement data. The displacement data are then further analyzed in both the time and frequency (i.e., power spectra density) domains.

Various materials have been previously used to demonstrate the diagnostic capabilities. For example, a 5-mm-thick copper disk was used (diameter of 45 mm) to demonstrate tracking of local temperature change.[27] In this case, the material choice reflects the need to maximize the energy absorption of the available heating laser. For that demonstration, the distance between the probe and sensor lasers is ∼6.7 mm with the heating laser approximately in the center. In an AM production tool, the laser beam wavelength could be optimized for the material in use. The reflectivity of copper at 488 (heterodyne sensor), 532 (green probe laser), and the 514 nm (heating laser) is 0.539, 0.659, and 0.601, respectively. Consequently, nearly half of the incident light is lost to reflection at all these wavelengths. For example, ∼58% of the heating laser is reflected, which limits the maximum temperature that could be achieved in this proof-of-principle demonstration. Other materials used are aluminum (bulk extruded) and Ti6Al4V.

3 Results

3.1 *Temperature Measurements*

SAWs can be used to measure a change in temperature within and around a heat-affected zone (HAZ). The prospect rests on the fact that the speed of sound is a function of temperature and in most materials, the sound velocity decreases with increasing temperature. Consequently, changes in the local temperature can be discernable by a change in the SAW arrival time. Its utility as a real-time, local temperature monitor in AM has been previously addressed.[27] Below, we present a simulation intended to demonstrate the feasibility of SAWs to characterize the size of an HAZ region and the cooling profile that surrounds the region. The simulation presumes an AM tool having pattern motion capability that is moderate-to-high speed (150 mm/s).

The change in the velocity of sound, which appears as a change in the SAW arrival time (or a "time delay" when compared with a reference), can described by the equation

$$t_d = t_0(1 + \alpha_T \Delta T), \tag{3}$$

where t_d is the time delay with respect to the time of travel t_0 at a reference temperature. ΔT is the temperature change with respect to the reference, and α_T is the temperature coefficient of delay.[29,30] This equation applies to a material volume with a homogeneous change in temperature.

As a function of time t and *x*-, *y*-, and *z*-coordinates, the temperature distribution for a Gaussian spatial profile laser beam moving across a material surface can be modeled with the following equation:[31,32]

$$T(t) - T_0 = \frac{q}{\pi \rho C (4\pi\kappa)^{1/2}} \int_0^{t_{\max}} \left[\frac{(t_{\max} - t)}{2\kappa(t_{\max} - t) + \sigma^2} \right.$$
$$\left. \times \exp\left\{ -\frac{(x - vt)^2 + y^2}{4\kappa(t_{\max} - t) + 2\sigma^2} - \frac{z^2}{4\kappa(t_{\max} - t)} \right\} \right] dt, \tag{4}$$

where q is the incident laser power, ρ is the density, C is the heat capacity, κ is the thermal diffusivity, σ is the beam radius, ν is the beam velocity along the propagating axis (e.g., *x*-axis), $t_{\max}$ is the time duration of the applied laser energy, and T_0 is the initial temperature of the material, respectively. The equations define an incident laser beam on the *x*-, *y*-planes with z defined as depth. When the z value is set to zero, the temperature distribution devolves into a two-dimensional (2-D) model and represents the

temperature profile on the surface, which to first order is an upper limit. At a particular time, t, Eq. (4) shows the change in temperature with respect to a reference value. Substituting Eq. (4) into Eq. (3) relates the SAW arrival time (i.e., delay) with thermal properties of the material [note: that t in Eq. (4) is time, whereas t_d in Eq. (1) is the delay time associated with SAW travel]. The simulation follows the methodology below:

- A surface region much larger than the anticipated HAZ and for specific time duration of travel is first defined (e.g., $x = 9$ and $y = 3$ mm).
- As a function of select times, the temperature distribution is calculated over the surface at select times.
- The surface temperature distribution is portioned into a mesh of 2-D squares, where the temperature within each square is assumed to be constant for the select times the calculation is derived.
- At specific distance increments across the laser beam travel direction, the SAW arrival time delay is calculated using Eq. (1) and the temperature difference between adjoining squares. The sum of these incremental time delays results in the total time delay experienced by the SAW.

- The temperature distribution is assumed to be frozen during the brief time it takes the SAW to propagate 3 mm. For example, in most metals the SAW velocities are ∼3 km/s and so the travel of 3 mm takes 1 μs. The thermal diffusivity of most metals is such that over 1-μs duration, heat transfer is on the order of 5 to 10 μm [Ref. 33 Prokhorov, Table 2.1]. Consequently, the change in the temperature distribution should be negligible for this analysis.

Details of the simulation include the heat input (35 W) applied by the CW laser, a laser beam radius of (150 μm), and the patterning velocity (150 mm/s along the Y-axis). We use material and thermal properties for steel. The thermal diffusivity is $\kappa = 5 \times 10^{-6}$ (m^2/s). The temperature coefficient of time delay is approximated[29] from velocity versus temperature curves for steel[34] and is set as 150 ppm/K.

Figure 2(a) shows the spatial distribution of the temperature after the laser has been on for a period of 0.05 s and has traveled 7.5 mm. The inset in Fig. 2(a) shows slices of this temperature distribution along the Y-axis (perpendicular to the travel path), with the highest temperature distribution slice representing the distribution at the current laser beam
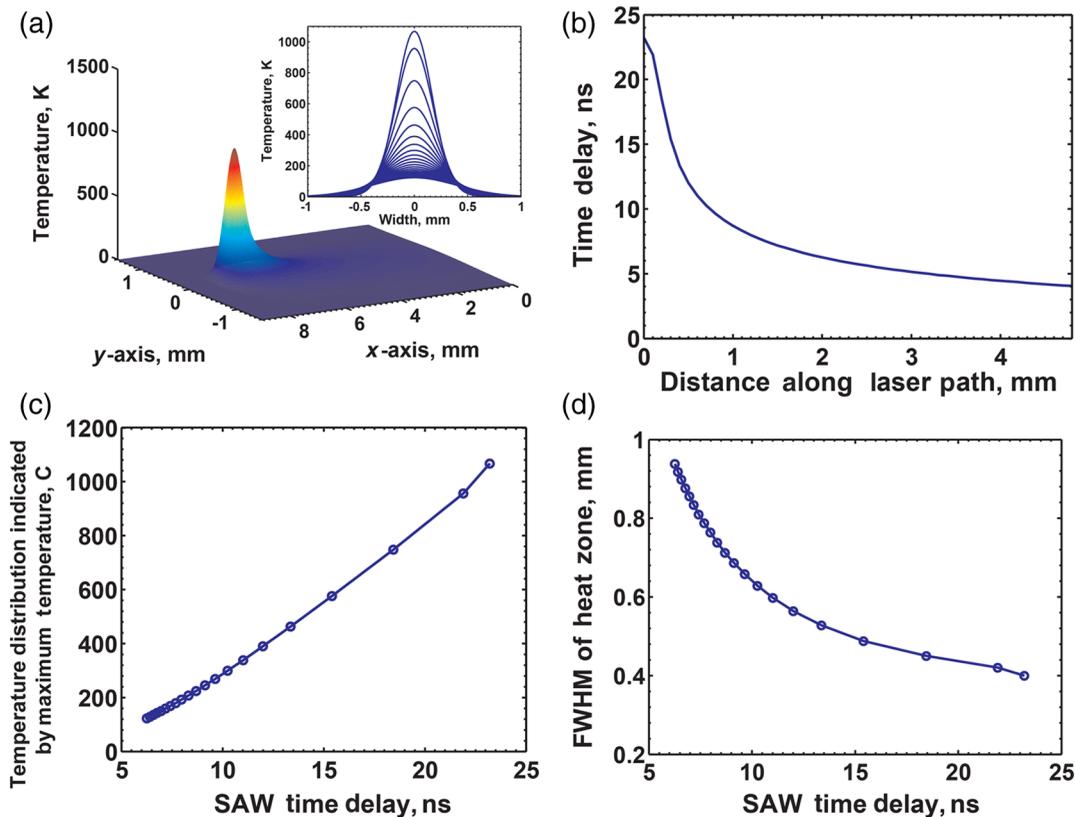

Fig. 2 (a) A simulation of the spatial distribution of the temperature from a moving (150 mm/s) CW laser incident on steel. Motion is along the x-axis. (a) Inset: Spatial distribution of the temperature along the y-axis starting at the center of the laser beam (top profile at $y = 0$ mm, $x = 8$ mm) and progressively further back along the traveled x-axis (successively lower amplitude curves) in increments of 0.1 mm. (b) The calculated SAW arrival time or delay (with respect to a reference) versus distance along the traveled path (0 mm represents the location of the laser beam center). (c) The arrival time or delay of an SAW packet that has propagated through a distribution as shown in Fig. 2(a) inset which has a maximum temperature defined by the Y-axis. (d) The FWHM (in mm) for the temperature distributions in Fig. 2(a) inset as a function of the SAW time delay. Data in (c) and (d) are plotted as a guide to the process engineer, who measures the SAW arrival time and can discern the maximum temperature along the path and FWHM of the HAZ.

location, followed by slices of the temperature distribution at sequential 0.1-mm increments along the beam path traveled. Figure 2(b) shows the calculated change in SAW arrival time or delay using Eq. (1) for the temperature distribution shown in Fig. 2(a) and a probe and sense laser beam separation of 3 mm (i.e., straddling the heating laser path). The calculated SAW delay times show that it is experimentally feasible to track the change in temperature of a fast-moving sintering laser. Figures 2(c) and 2(d) show the simulated results in a format that would be useful to a process control engineer. The figures show the estimated maximum temperature along the SAW path and the extent of the HAZ (FWHM) along that path. Consequently, by tracking the SAW arrival time or delay, a near-real-time monitor of the maximum temperature (along the path) and the extent of HAZ can be had. With multiple probe and sense beams, where each pair is separated by a nominal distance (e.g., 0.1 to 0.2 mm) along pattern laser path and the SAW pulses are applied in a sequence, it would be possible to measure the maximum temperature along a laser travel path and thus the "cooling rate" along the path as shown in Fig. 2(a).

Melting and heating in real AM processes with powdered metals often produce higher temperatures, larger heating areas, and temperatures that can persist for longer periods than those modeled here. Moreover, with higher fidelity

analysis of the time-dependent signal, it may even be possible to capture information on material property changes (elastic and inelastic).[35] For example, phase changes during heating and cooling can be reflected in time-delay plots and may appear as significant deviations from the calculated results.

3.2 In Situ Diagnostics on Sharp Radii Curved Surfaces

There are fabrication processes where monitoring a material property along a sharp curved surface can be useful, for example, in wire fed electron beam AM or electron beam freeform fabrication.[36,37] In wire fed and extruded material deposition processes, the feedstock material typically has some curvature (e.g., 1 to 4 mm dia. for some tools). An *in situ*, noncontact, diagnostic that monitors properties (e.g., local temperature and roughness) would be helpful. The diagnostic would be placed on the feedstock material near the melting point or at the location where the melted material begins to fuse to the under layer below. The concept of laser SAW as a diagnostic on curved surfaces is presented using a large diameter sample and a thin wire sample [see Fig. 3(a): bottom right photo]. A curved Ti6Al4V sample is milled down from a rod to ~1-cm diameter. The sample is mounted such that the probe laser beam, in this case
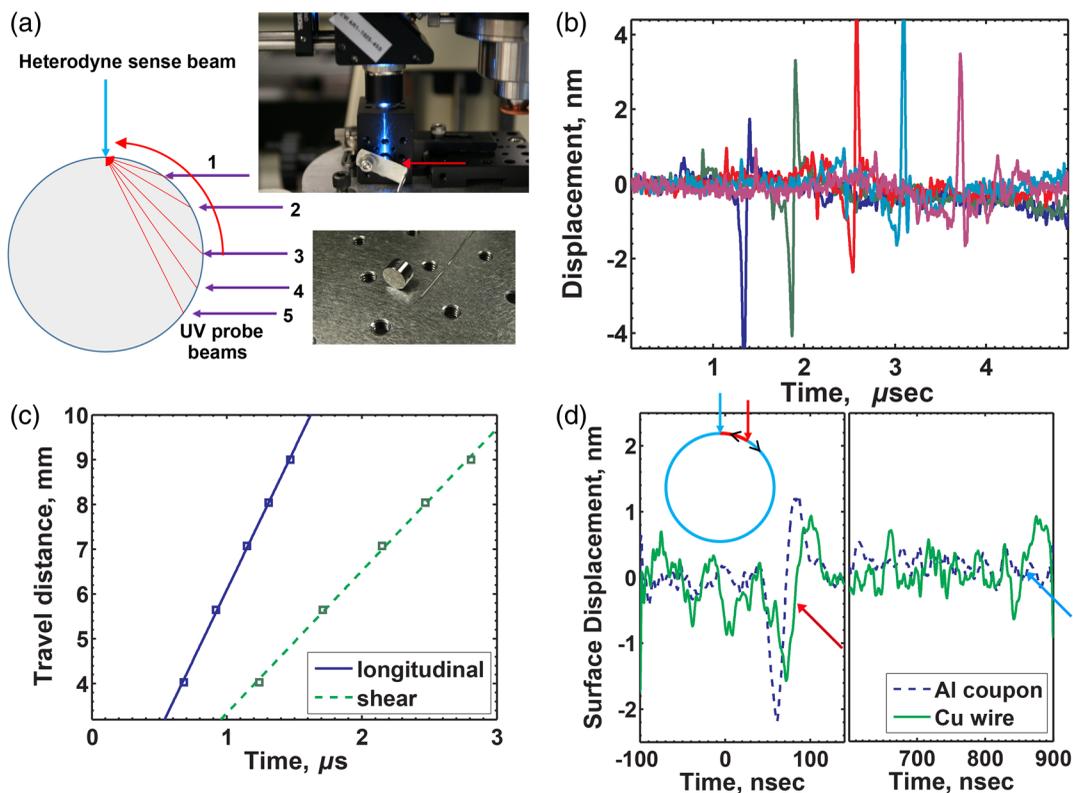

Fig. 3 (a) Right: Probe–sense configuration applied to cylindrical sample and a photograph of the 1-cm dia. sample and 650-μm dia. wire. Left: schematic depicting the measured locations of the probe and sense beams. (b) Measured displacement as a function of arrival time for the SAW mode. (c) Plot of the calculated travel distance versus measured arrival time of the bulk wave modes (longitudinal and shear). The slope defines the speed of sound for the wave mode. (d) Plot of the surface displacement versus arrival time of a reference material (aluminum flat coupon) and a 650-μm dia. copper wire. The $t = 0$ defines the initiation of the probe laser pulse. Two SAW mode pulses (depicted by arrows) are identified for the case of the cylindrical wire. The early arrival time represents an SAW mode that has traveled a short distance, whereas the late arrival time signal is a wave that has propagated in the opposite direction in relation to the first. The inset depicts the counter propagating waves.

a pulsed UV laser, is incident horizontally and the sensor laser is directed downward at a 90-deg angle to the probe laser beam [see Fig. 3(a): top right photo]. The probe laser beam is shaped to a line focus with dimensions of (2 to 3 mm × 50 to 100 microns).

Data are collected using the acquisition approach as shown in Fig. 1 except that the measured signals are distinguished, by their arrival time, into the three primary wave modes such as the SAW, the longitudinal, and shear waves. The latter wave modes are also called bulk modes because they travel through the material. Data are taken at five probe-to-sensor distances as shown in Fig. 3(a) sketch. The arrival time of the SAW mode from the five locations is shown in Fig. 3(b), which is a plot of the surface displacement as a function of time. Simple geometry is used to derive the perimeter distance that would be the path of the SAW wave, whereas the chord would be one possible path for the longitudinal and shear modes. For example, using the calculated distance between probe-to-sensor, where the probe is at location 3 [Fig. 3(a)] along with the measured arrival time (2.537 μs), yields a value of 3113 m/s for the SAW velocity that is close to that in the literature for Ti6Al4V.[38,39]

The identification and characterization of the shear and longitudinal waveforms provide additional evidence because these modes travel along the chord and provide information buried within the sample. Figure 3(c) shows a plot of the calculated travel distance versus the measured arrival times. The velocity is derived from the slope. Fitting the data shows a longitudinal wave mode velocity of 6280 m/s, which is within 4% of the literature value.[39] Similarly, the shear wave mode velocity, from the fit, is 3174 m/s, which is within 3% of the literature value.[39] One of the advantages of the presented diagnostic over optical emission diagnostics is the utility of ultrasound waves as probes for subsurface material properties. For example, if the longitudinal and/or shear modes do not appear, one can suspect empty pocket defects, or if the velocity of these modes do not conform to establish values for the speed of sound, one can suspect other alloys to have formed.

Figure 3(d) shows the results from a tinned copper wire 650 μm in diameter [shown in Fig. 3(a) photo on lower left] and a flat aluminum sample used as a reference. The plot shows the measured surface displacement as a function of time. A probe-to-sensor distance of 200 μm is used. The distance length is corroborated by measuring the SAW mode arrival time from a flat aluminum sample, where the speed of sound of the SAW mode is known (dashed line). The copper wire data (solid line) shows two features identified by arrows. The feature with the higher signal-to-noise ratio is a wave that has traveled a short distance to the sensor, whereas the latter arriving feature corresponds to the SAW mode that has circumnavigated around the whole wire. Both SAWs have travel times that are expected with copper. The inset in Fig. 3(d) shows the two-wave modes. These results demonstrate that SAW modes measured at a nm level of displacement can be used to measure surface properties of a small diameter wire. The use of the aluminum SAW to verify probe–sense distance also acts as a verification for the technique (i.e., measuring properties on small curved samples), though the SAW from an aluminum flat surface is measured. Prior knowledge of the propagation of SAWs

Table 1 Calculated arrival times for acoustic waves incident on 50-μm radius bump.

	Circumference	Bulk
	78.5 microns	70.7 microns
SAW	25.2 ns	—
Shear	—	22.3 ns
Longitudinal	—	11.3 ns

on flat aluminum ensures that short probe-to-sense distance is operable. Although there may be some potential for slight dispersion of SAWs on curved surfaces,[40,41] the results of the travel distances and arrival times help qualify the accuracy of the measurements and bring support to the technique.

It is possible to estimate the curvature limit that can be measured based on our existing experimental capabilities, which use 3- to 10-ns pulse width lasers. The measurement of small radius of curvature becomes easier, the shorter is the pulse width laser (e.g., femtosecond laser can generate submicron wavelength SAWs). Also, with a decrease in the radius of curvature there is a concomitant reduction in the arrival time between the bulk and SAW modes. However, with detailed analysis and possible use of machine learning algorithms, signal shape changes can be distinguished and characterized to separate a bulk mode from an SAW mode. For example, consider a probe laser that is incident on top of a 50-μm radius bump above a Ti6Al4V surface. The travel distance from the top to the edge along the surface is 78.5 μm, whereas a bulk wave traveling along the chord is 70.7 μm. Table 1 shows the calculated arrival times for a sensor beam placed at the edge for the bulk and surface wave modes. This appears to be close to the limit of our capability using a 3-ns pulse width laser and diagnostics with time resolution limit of ∼5 ns.

3.3 Near-Real-Time Qualitative Measurement of Surface Roughness

Surface roughness plays a key role if a high-quality, layer-by-layer build is desired. A diagnostic that can qualitatively monitor the surface roughness at each layer without adding significant time to the overall AM process would be valuable. The measurement could enable a corrective action to be applied locally to smooth out a roughened section (e.g., a second laser or e-beam pass). The ability to use SAWs to investigate surface roughness, as well as microstructure, surface defects, and subsurface defects, is related to the scattering and attenuation of SAWs in the presence of these features.[14,15,17,42] We demonstrate the diagnostic technique as a surface roughness monitor here.

The experiment uses an NIST-traceable surface roughness comparator (GAR Electroforming E-9 Electrical Discharge Machined Microfinish Comparator) as the reference standard. The SAW signals are analyzed by an algorithm that compares the surface microfinish with the NIST standard, on the scale of 0.5 to 5 μm (i.e., subparticle grain size). Figure 4(a) shows a photograph of the surface roughness comparator with R_a values (arithmetical mean) as defined by Eq. (3), where y_i represents a measured height
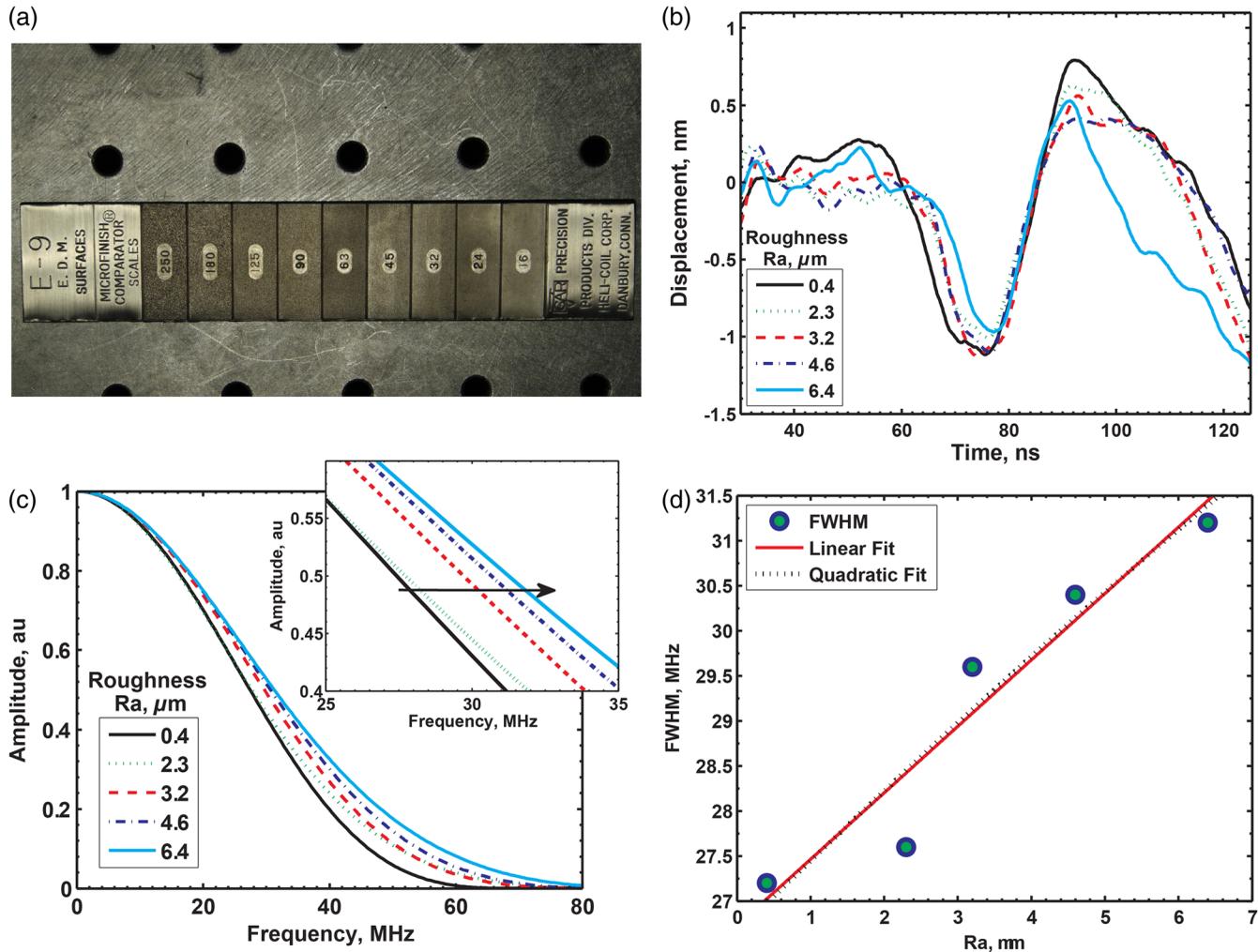
(a)

(b)

(c)

(d)

Fig. 4 (a) GAR Electroforming E-9 electrical discharge machined microfinish comparator used for surface roughness evaluation. (b) Displacement versus time for SAWs measured over different roughness regions. (c) Frequency distribution (normalized with respect to the maximum) for the SAW waves measured over different surface roughness regions. (d) Frequency at the FWHM for the frequency distributions over each surface roughness region.

$$R_a = \frac{1}{n} \sum_{i=1}^{n} |y_i|. \qquad (3)$$

The R_a values on the reference vary from 0.4 to 6.4 microns. Laser SAWs are produced, measured, and analyzed at several locations on the comparator standard simply by positioning the probe and sense lasers at arbitrary locations within different roughness regions. Data are collected for roughness areas with R_a ranging from 0.4, 2.3, 3.2, 4.6, and 6.4 microns (or 16, 90, 125, 180, and 250 microinches), respectively. The probe and sensor lasers are always separated by a distance of ~110 microns, which defines the nominal measured area. Figure 4(b) shows the time-resolved surface displacement data containing the SAWs (50- to 100-μs portion) measured for each roughness region, with the primary observable being a decrease in the pulse width of the main negative-going SAW pulse. The trend is more obvious in the data of Fig. 4(c), which is a normalized frequency spectrum of the data in Fig. 4(b) and suggests a trend that with increasing R_a, the FWHM of the frequency spectrum grows. This trend is more obvious in Fig. 4(d),

where the value of the FWHM is plotted as a function R_a. Linear and quadratic fits are applied to capture the trend shape. The resulting trend demonstrates a potentially simple method for qualitatively estimating changes in the surface roughness during *in situ* process monitoring. A simple FFT can be done on the time-resolved signal and the value compared with a standard. To further expedite near-real-time analysis, one may need not compute the full discrete Fourier transform and approximations may suffice.[43] In powder bed AM tools, powder diameters vary from 5- to 20-microns, one would expect a well-sintered surface layer to have roughness <5 microns and preferably <0.5 microns.[44] Consequently, our diagnostic technique demonstrates that it may be possible to institute a R_a "out of range" condition along the build layer with measured segments as short as 110 microns apart.

3.4 Utility as a Transient Diagnostic to Identify Solitary Defects on the Order of 10 μm

Surface roughness (i.e., R_a) is a descriptor of the variation in surface feature height; it describes the deviations of the

normal vector of the real surface from its ideal form. Although it is a necessary parameter to monitor, it usually does not encompass the existence of solitary defects, such as a small surface indentation left from an unmelted powder grain that has been brushed away. This form of defect, although minute (<20 microns), does appear in AM processing and results in the possible formation of a buried defect if not repaired. If such defects can be identified between layering operations, then one can envision a process for locally repairing it (e.g., filling the "potholes" on a street prior to resurfacing). Therefore, a diagnostic that identifies "solitary" defects is also necessary in addition to one that measures R_a.

The identification of solitary defects requires an analysis of the time-dependent signals slightly different from one that diagnoses the qualitative R_a value. An experiment has been done to explore whether solitary defects (i.e., on the scale powder grain size or 10 microns) can be teased out from the time-dependent signal. As a means to demonstrate the diagnostic, a sample with a square array of 10- to 20-micron diameter holes (i.e., pits) is prepared by pulsed laser ablation. Figure 5(a) shows an optical microscope image of one such "defect." The defects are spaced 150 microns apart on an

aluminum 6061 sample. The probe–sense beams are aligned such that the UV probe and sensor laser beams straddle the defect. This would be the nominal diagnostic configuration within an AM tool as collinear probe and sensor beams are made to scan along a build layer. It is important to point out, at this juncture, the advantage of laser-induced SAWs in comparison with traditional piezoelectric-generated SAWs. In the former case, the generated SAWs have wide bandwidth (∼$1/\tau$, where τ is the pulse width of the laser, e.g., 1 ns?1 GHz while piezoelectric materials, because of the nature of crystalline matter, "ring" with narrower bandwidth. The implication is that for the case of the laser-generated waves, the propagating wave packet can contain shorter wavelengths ($\Lambda = V/f$ where Λ is the wavelength, V is the velocity of sound, and f is the frequency). Scattering theory argues that wave disturbance becomes more efficient when the size of the scattering center approaches the wavelength of the wave being scattered.[15] Figure 5(a) shows the track of the probe laser along a line of defects. The visible track is not ablated material but a discoloration caused from reaction with oxygen because the experiment was not done in an inert atmosphere. The sensor beam, which has even
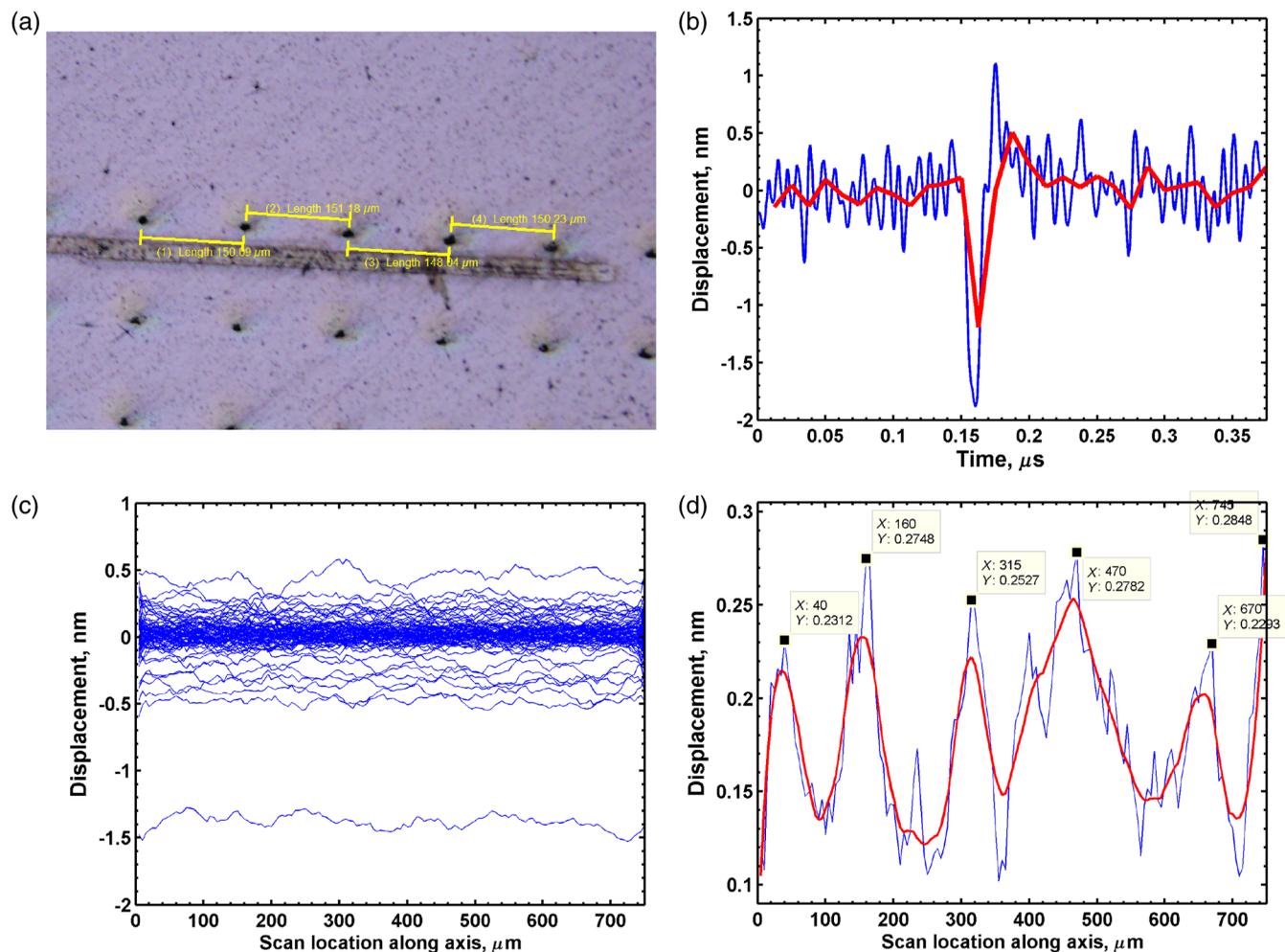

Fig. 5 (a) Pre-fabricated square array of 10- to 20-μm size holes separated by 150 microns in each direction. (b) SAW curve of a single probe–sense signal located at some location along the scan direction. (c) The displacement (itself a function of the time) versus the location along the scan axis. Each blue curve represents a different time point during recording of the surface measurements. (d) Filtering and peak extraction of a single displacement versus scan location curve.

lower power does not leave a visible impression and in this configuration, is located above the track line of defects. The probe–sensor separation is ~115 μm and data are acquired in 10-μm stage motion increments. The surface displacement signal from a single SAW pulse at an arbitrary location along the track is shown in Fig. 5(b) after signal processing. In our experiment, we are limited by the repetition rate of our laser (100 Hz). Data can be acquired far more quickly using a higher repetition rate laser (kHz-MHz). A data processing algorithm has been developed that implements Savitzky–Golay filtering (blue curve),[45] followed by time binning (red curve). Figure 5(c) shows the amplitude of the algorithm-processed-signal from 150 measured locations and at different time segments. Many of the values reside on or near zero displacement. Those traces are not further analyzed. However, of the nonzero displacement traces (for example, the second curve down from the highest curve) additional filtering analysis is done. Figure 5(d) shows the results of the filtered data plotted as a function of track distance. The trace is highlighted by peaks that correspond with the locations of the defects along the scan direction. Using a peak extraction algorithm, we deduce an average peak separation distance of 151.7 μm. This value is within 2 μm from the known defect separation distance of 150 μm. Moreover, we believe there is more information in Fig. 5(d) data. For example, the slope to either side of the peak location identifiers could be a representative effect of the defect diameter. Further experiments are necessary to confirm this observation. Regardless, these results show strong promise for *in situ* detection of solitary defects on the order of powder grain size (10 to 20 μm). The method is extensible to identifying subsurface defects[46] and our laboratory has used a more traditional ultrasound NDE technique to image weld properties of two metal sheets.[47,48]

4 Outstanding Issues and Other Approaches

The results show that laser ultrasonics coupled with laser heterodyne displacement sensing provides the means for an *in situ* monitoring technique from which several key processing parameters relevant to AM can be derived. The technique may also find use in other manufacturing technologies. Although the technique shows promise, there are issues yet to be addressed. For example, in these proof-of-principle demonstrations, a specific probe–sensor configuration is used to derive the process parameter of interest. To limit the proliferation of diagnostic probes, it would be more sensible if the deduction of multiple process parameters could be demonstrated from a single measurement. On the other hand, the technique is laser based (i.e., nonintrusive) and multiple probe–sensor systems could easily be implemented within a commercial tool. Each configuration can then be dedicated to addressing a specific parameter and time synchronization of the pulsed probes limits signal cross talk among the multiple sensor channels. Another important process parameter is knowledge of the grain size of the sintered material during the build. Grain size affects mechanical and fatigue properties of materials and, to some extent, can be controled by the cooling rate. Consequently, a measurement of the cooling rate near the sintered region could be one indirect approach to monitoring microstructure. One can envision a set of probe–sensor laser combinations that monitor the local temperature at specific

locations away from the sintered matter. The process control protocol would entail monitoring of cooling profile to yield the desired microstructure. A direct measurement of the grain size, grain boundary, and grain orientation has been reported by laser ultrasonic methods.[49,50] These techniques apply structured light (i.e., patterned light) to induce a narrow frequency bandwidth SAW and then track the change in the bandwidth when crossing grain boundaries. Preliminary results within our own lab show that this approach has utility and, when combined with broadband laser ultrasonic techniques, could yield a wide range of analysis approaches for AM. It does, however, rely on computational processing power and this could limit fabrication speed.

Residual stress is another property that has been characterized by SAW arrival times analysis.[16,51] Residual stress, on the order of 300 MPa, can change SAW velocities by tens of m/s or a ~1% change.[51] The velocity of an SAW in the same material, but along different grain orientations, can vary by as much as 100 m/s or more.[52] Consequently, distinguishing residual stress from a grain boundary crossing poses challenges that require further experimentation. But, we note that these phenomena add potential error to the diagnostics as presented. We repeat that the intent is not to measure absolute values but to develop a methodology that combines *in situ* sensing coupled with fast analysis to yield a process control system that can be used to maintain the build within a defined process "window."

Other laser-based techniques exist, which may also prove to be useful. For example, the analysis of speckle produced by a sensor laser scattering off the surface could provide information on surface roughness.[53,54] Another approach is to apply direct interferometry via a two-wave mixing in photorefractive materials.[55–57] Many of these approaches may provide the necessary information for maintaining process control but at a cost of further complexity (computation and/or hardware). This must be balanced with the fidelity and speed of the information that can be derived from the signals. By its very nature, AM is a serial process and any diagnostic that further slows fabrication speed is not likely to be useful from an industrial perspective. In contrast, and this will depend on the application, industry may well make allowances for time spent to make local repairs to guarantee a "defect"-free part. To at least first order, process control systems must maintain speeds commensurate with current build times.

5 Conclusion

In a series of experiments, we have demonstrated that combining the laser ultrasonic method with laser heterodyne displacement sensing enables the monitoring of local changes in the surface temperature, a measurement of the extent of the HAZ, a qualitative sense of changes in the surface roughness, and the identification of solitary defects. Moreover, we have also demonstrated its utility for monitoring property changes on curved surfaces with small radii. Based on our experimental arrangement, we deduce it is possible to monitor around a curved surface with radii of <100 μm. All the diagnostic approaches are intended to provide relative data primarily for process monitoring. The relative data can be made absolute given a set of calibration curves or lookup tables for comparison. The technique has the following advantages: (1) it is possible to select a signal mode, where the

measurement is at the surface because the energy resides at the surface interface (e.g., SAW mode), or in layers below (e.g., bulk modes). With pulsed laser ultrasonics, where the bandwidth of ultrasonic pulses is wide, one is afforded a further diagnostic refinement, the ability to monitor properties as a function of depth. SAW modes penetrate approximately one to two wavelengths deep. Consequently, frequency filtering of an SAW packet contains information as a function of depth. (2) Time synchronous initiation coupled with data acquisition can be used to capture information at a moment in time and location. This enables the multiplexing of multiple probe–sense laser diagnostics, each probing a different property. (3) The method (hardware + analysis software) has potential applicability in other forms of manufacturing processes beyond that of AM, such as *in situ* and nonintrusive testing of work pieces that are undergoing fatigue and cycle testing, or in a postfabrication process, where the work piece surface is being modified (e.g., laser hardened). A summary of the capabilities as follows:

- The technique is a noncontact approach providing information between the probe and sensor locations.

- Both the probe and sensor are laser-based. Consequently, they can be rapidly positioned with automated galvo scanners.

- The diagnostic can provide information on local temperature and microstructure, on demand.

- The use of time-resolved measurement (resolution 10^{-9} s) enables faster analysis and possibly finer resolution of material properties.

- The sensitivity of the diagnostic can be further enhanced by matching the probe and sensors laser wavelength to the material absorption properties.

- The diagnostic works on reflective materials and with more complex analysis also in translucent materials.

- By calibrating the diagnostic to absolute temperature, it may also allow the tracking of a phase transformation, e.g., as the material cools.

- Finally, the diagnostic can also be used as a, nonstylus, surface profilometry tool with nm vertical resolution.

Acknowledgments

References

1. W. Chen et al., "Direct metal writing: Controlling the rheology through microstructure," *Appl. Phys. Lett.* **110**, 094104 (2017).
2. A. Jabbari and K. Abrinia, "A metal additive manufacturing method: semi-solid metal extrusion and deposition," *Int. J. Adv. Manuf. Technol.* **94**, 3819–3828 (2018).
3. J. Mireles et al., "Fused deposition modeling of metals," in *The Twenty-Third Annual Int. Solid Freeform Fabrication (SFF) Symp.* (2012).
4. D. D. Gu et al., "Laser additive manufacturing of metallic components: materials, processes and mechanisms," *Int. Mater. Rev.* **57**(3), 133–164 (2012).
5. J. P. Kruth et al., "Selective laser melting of iron-based powder," *J. Mater. Process. Technol.* **149**(1–3), 616–622 (2004).
6. Z. Y. Chua, I. H. Ahn, and S. K. Moon, "Process monitoring and inspection systems in metal additive manufacturing: status and applications," *Int. J. Precis. Eng. Manuf.-Green Technol.* **4**(2), 235–245 (2017).
7. T. G. Spears and S. A. Gold, "In-process sensing in selective laser melting (SLM) additive manufacturing," *Integr. Mater. Manuf. Innov.* **5**(1), 2 (2016).
8. S. K. Everton et al., "Review of in-situ process monitoring and in-situ metrology for metal additive manufacturing," *Mater. Design* **95**, 431–445 (2016).
9. F. E. Livingston and H. Helvajian, "Laser processing architecture for improved material processing," Chapter 13 in *Laser Processing of Materials*, P. Schaaf, Ed., pp. 189–224 Springer-Verlag, Berlin Heidelberg (2010).
10. J. L. Rose, *Ultrasonic Guided Waves in Solid Media*, Cambridge University Press, New York (2014).
11. P. Hess, "Surface acoustic waves in materials science," *Phys. Today* **55**(3), 42–47 (2002).
12. H. Yamada, A. Kosugi, and I. Ihara, "Noncontact monitoring of surface temperature distribution by laser ultrasound scanning," *Jpn. J. Appl. Phys.* **50**(7), 07HC06 (2011).
13. E. Fraizier, M. H. Nadal, and R. Oltra, "Evaluation of viscoelastic constants of metallic materials by laser-ultrasonics at elevating temperature," *Ultrasonics* **40**(1–8), 543–547 (2002).
14. V. V. Kosachev, Y. N. Lokhov, and V. N. Chukov, "Theory of attenuation of Rayleigh surface acoustic waves on a free randomly rough surface of a solid," *Sov. Phys. JETP* **67**(9), 1825–1830 (1988).
15. E. P. Papadakis, "Ultrasonic attenuation caused by scattering in polycrystalline metals," *J. Acoust. Soc. Am.* **37**(4), 711–717 (1965).
16. A. Moreau, "Laser-ultrasonic characterization of the microstructure of aluminum," *Mater. Sci. Forum* **519**–**521**, 1373–1378 (2006).
17. B. Masserey and E. Mazza, "Ultrasonic sizing of short surface cracks," *Ultrasonics* **46**(3), 195–204 (2007).
18. R. E. Lee and R. M. White, "Excitation of surface elastic waves by transient surface heating," *Appl. Phys. Lett.* **12**(1), 12–14 (1968).
19. K. Murakami et al., "Time-resolved and space-resolved Si lattice-temperature measurements during CW laser annealing of Si on sapphire," *Appl. Phys. Lett.* **45**(6), 659–661 (1984).
20. J. Z. Tischler, B. C. Larson, and D. M. Mills, "Time-resolved x-ray study of Ge during pulsed laser melting," *Appl. Phys. Lett.* **52**(21), 1785–1787 (1988).
21. D. E. Hare, J. Franken, and D. D. Dlott, "Coherent Raman measurements of polymer thin-film pressure and temperature during picosecond laser-ablation," *J. Appl. Phys.* **77**(11), 5950–5960 (1995).
22. S. Namba et al., "Surface temperature of metals heated with laser," *Jpn. J. Appl. Phys.* **4**(2), 153–154 (1965).
23. P. Hermes et al., "Evaporation of atoms from femtosecond laser-heated gallium-arsenide," *Appl. Phys. A* **39**(1), 9–11 (1986).
24. G. V. Sergienko, G. I. Stotsky, and N. M. Zykova, "Measurement of the target surface-temperature in the presence of a laser-induced plasma," *Meas. Sci. Technol.* **5**(12), 1448–1452 (1994).
25. H. E. Elsayedali and J. W. Herman, "Picosecond time-resolved surface-lattice temperature probe," *Appl. Phys. Lett.* **57**(15), 1508–1510 (1990).
26. D. Otte, H. Kleinschmidt, and O. Bostanjoglo, "Space and time resolved temperature measurements in laser pulse-produced metal melts," *Rev. Sci. Instrum.* **68**(6), 2534–2537 (1997).
27. A. J. Manzo and H. Helvajian, "Pulsed laser ultrasonic excitation and heterodyne detection for in situ process control in laser 3D manufacturing," *J. Laser Appl.* **29**(1), 012012 (2017).
28. J. F. Ready, *LIA Handbook of Laser Materials Processing*, Magnolia Publishing, Inc., Orlando, Florida (2001).
29. A. J. J. Slobodnik, "Materials and their influence on performance," in *Acoustic Surface Waves*, A. A. Oliner, Ed., pp. 285–289, Springer-Verlag, Berlin, Germany (1978).
30. M. Y. Dvoesherstov et al., "The temperature coefficients of delay of surface acoustic waves in LGS and LGN crystals in a wide temperature range," *Tech. Phys.* **46**(3), 346–347 (2001).
31. H. E. Cline and T. R. Anthony, "Heat treating and melting material with a scanning laser or electron-beam," *J. Appl. Phys.* **48**(9), 3895–3900 (1977).
32. T. W. Eagar and N. S. Tsai, "Temperature-fields produced by traveling distributed heat-sources," *Weld. J.* **62**(12), S346–S355 (1983).
33. A. M. Prokhorov et al., *Laser Heating of Metals*, IOP Publishing Ltd., Bristol (1990).
34. B. Hutchinson et al., "Anomalous ultrasonic attenuation in ferritic steels at elevated temperatures," *Ultrasonics* **69**, 268–272 (2016).
35. M. Paul, B. Haberer, and W. Arnold, "Materials characterization at high-temperatures using laser ultrasound," *Mater. Sci. Eng. A* **168**(1), 87–92 (1993).
36. P. E. Wollenhaupt and S. Stecker, "Raster methodology, apparatus and system for electron beam layer manufacturing using closed loop control," U.S. Patent No. 9174300B2 (2013).
37. K. M. Taminger and R. A. Hafley, "Electron beam freeform fabrication for cost effective near-net shape manufacturing," Technical Memorandum, NASA/TM-2006-214284, NASA (2006).
38. S. Sathish and R. W. Martin, "Quantitative imaging of Rayleigh wave velocity with a scanning acoustic microscope," *IEEE Trans. Ultrason. Ferroelectr. Freq. Control* **49**(5), 550–557 (2002).

39. E. R. Naimon, W. F. Weston, and H. H. Ledbetter, "Elastic properties of two titanium alloys at low temperatures," *Cryogenics* **14**, 246–249 (1974).
40. D. Royer and D. Clorennec, "Theoretical and experimental investigation of Rayleigh waves on spherical and cylindrical surfaces," in *1st Int. Symp. on Laser Ultrasonics: Science, Technology and Applications*, Montreal, Canada (2008).
41. D. Clorennec and D. Royer, "Analysis of surface acoustic wave propagation on a cylinder using laser ultrasonics," *Appl. Phys. Lett.* **82**(25), 4608–4610 (2003).
42. H. Cho, S. Ogawa, and M. Takemoto, "Non-contact laser ultrasonics for detecting subsurface lateral defects," *NDT&E Int.* **29**(5), 301–306 (1996).
43. H. Guo and C. S. Burrus, "Fast approximate Fourier transform via wavelets transform," *Proc. SPIE* **2825**, 250–259 (1996).
44. E. Abele and M. Kniepkamp, "Analysis and optimisation of vertical surface roughness in micro selective laser melting," *Surf. Topogr. Metrol. Prop.* **3**(3), 034007 (2015).
45. A. Savitzky and M. J. E. Golay, "Smoothing and differentiation of data by simplified least squares procedures," *Anal. Chem.* **36**(8), 1627–1639 (1964).
46. L. W. Zachary, "Quantitative use of Rayleigh waves to locate and size subsurface holes," *J. Nondestr. Eval.* **3**(1), 55–63 (1982).
47. H. Hatano et al., "Mid IR pulsed light source for laser ultrasonic testing of carbon-fiber-reinforced plastic," *J. Opt.* **17**(9), 094011 (2015).
48. G. A. Gordon, S. Canumalla, and B. R. Tittmann, "Ultrasonic C-scan imaging for material characterization," *Ultrasonics* **31**(5), 373–380 (1993).
49. S. D. Sharples, M. Clark, and M. G. Somekh, "Spatially resolved acoustic spectroscopy for fast noncontact imaging of material microstructure," *Opt. Express* **14**(22), 10435–10440 (2006).
50. R. J. Smith et al., "Spatially resolved acoustic spectroscopy for rapid imaging of material microstructure and grain orientation," *Meas. Sci. Technol.* **25**(5), 055902 (2014).
51. A. Karabutov et al., "Laser ultrasonic diagnostics of residual stress," *Ultrasonics* **48**(6–7), 631–635 (2008).
52. S. Sathish et al., "Elastic-constants and crystal orientation of individual grains of polycrystalline solids from scanning acoustic microscopy," *J. Acoust. Soc. Am.* **98**(5), 2854–2857 (1995).
53. R. Lu, J. J. Koenderink, and A. M. L. Kappers, "Surface roughness from highlight structure," *Appl. Opt.* **38**(13), 2886–2894 (1999).
54. S. L. Toh, H. M. Shang, and C. J. Tay, "Surface-roughness study using laser speckle method," *Opt. Laser Eng.* **29**(2–3), 217–225 (1998).
55. R. K. Ing and J. P. Monchalin, "Broad-band optical-detection of ultrasound by 2-wave mixing in a photorefractive crystal," *Appl. Phys. Lett.* **59**(25), 3233–3235 (1991).
56. B. F. Pouet et al., "Heterodyne interferometer with two-wave mixing in photorefractive crystals for ultrasound detection on rough surfaces," *Appl. Phys. Lett.* **69**(25), 3782–3784 (1996).
57. M. B. Klein et al., "Homodyne detection of ultrasonic surface displacements using two-wave mixing in photorefractive polymers," *Opt. Commun.* **162**(1–3), 79–84 (1999).

Biographies for the authors are not available.